Gating Current Noise Produced by Elementary Transitions in *Shaker* Potassium Channels

Daniel Sigg, Enrico Stefani, Francisco Bezanilla*

Gating currents provide a direct record of the spatial rearrangement of charges occurring within the protein of voltage-sensitive ion channels. If the elementary charges move as very brief discrete pulses of current, they will produce fluctuations in the macroscopic gating current. The variance of such fluctuations in gating currents was measured in *Shaker* potassium channels expressed in *Xenopus* oocytes with a sufficiently high recording bandwidth to estimate the magnitude and time distribution of the elementary transition charge movements. Channel activation occurred in two sequential stages. The first stage consisted of numerous, fast transitions, each moving small amounts of charge that contributed little to the fluctuation in gating current, whereas the second stage, which contributed the bulk of the fluctuation, was represented by a number of discrete, correlated transitions, one or more of which carried a charge of at least 2.4 elementary charges across the membrane field.

Voltage-gated ion channels (*1*) are transmembrane proteins that, when activated by a change in voltage, undergo conformational changes leading to pore opening. Gating currents (*2*), which are the electrical manifestation of these conformational changes, arise from the movement of charged or dipolar residues intrinsic to the channel during transitions between states (Fig. 1A). The channel protein may pass from the initial closed to the final open state through an almost infinite number of states, like a diffusion process governed by Brownian motion, or may have abrupt and discrete changes in conformation that lead to distinguishable conformational states (*3*). The movements of charge occurring during these transitions are expected to occur as current impulses ("shots") (*4*) that should generate fluctuations in gating current recordings (*5, 6*). Although the elementary shot charge movement cannot be measured directly with available instrumentation, information can be obtained on its size and time distribution from the analysis of fluctuations in macroscopic gating currents induced by the elementary gating events, as was reported for sodium channels (*5*). We report the recording of fluctuations in the gating charge movement of *Shaker* potassium channels. The results confirmed the presence of discrete charged transitions in the channel protein during activation. An estimate was made of the elementary charge movement in one of those transitions as well as its relative position in the activation sequence.

The gating current from a single channel would appear as a series of impulses weighted by the effective charge moved (*7*) as shown in trace B1 of Fig. 1. Under recording conditions the impulses would be spread out by the filter, as shown in traces B2 and B3 of Fig. 1. If the average time between successive transitions (determined by the transition rates) is sufficiently low compared to the response time of the filter (high bandwidth condition), resolution of the individual events could be achieved (Fig. 1, B2). However, background noise limitations of current instrumentation prevent recording "shot" events from single channels, which are predicted to measure about 1 fA per elementary charge moved when recording with an 8-kHz filter. Nonetheless, information about the size and time distribution of single channel gating currents is obtainable through the analysis of nonstationary noise from an ensemble of macroscopic currents (*8*), provided that fluctuations are large enough to be resolved. By measuring the gating current noise of K^+ channels (decay time of 1 to 2 ms) at 17°C and 8-kHz bandwidth, we improved temporal resolution by an order of magnitude over previous measurements done on the faster Na^+ channels (*5*), allowing us to better distinguish the size and time dependence of gating charge movement during activation. To measure gating currents (*9*), we used a variant of the *Shaker* channel with a point

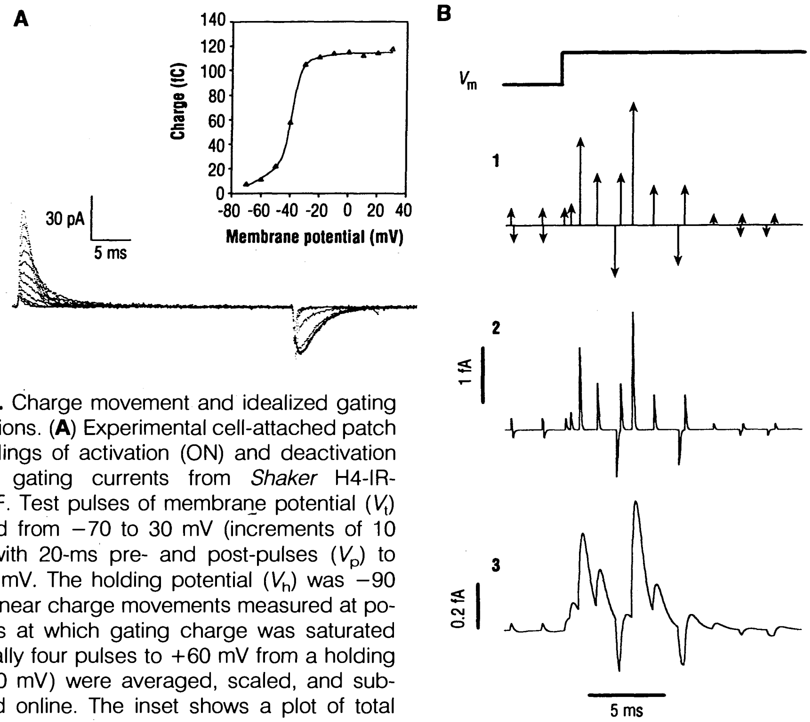

Fig. 1. Charge movement and idealized gating transitions. (**A**) Experimental cell-attached patch recordings of activation (ON) and deactivation (OFF) gating currents from *Shaker* H4-IR-W434F. Test pulses of membrane potential (V_t) ranged from −70 to 30 mV (increments of 10 mV) with 20-ms pre- and post-pulses (V_p) to −110 mV. The holding potential (V_h) was −90 mV. Linear charge movements measured at potentials at which gating charge was saturated (typically four pulses to +60 mV from a holding of +30 mV) were averaged, scaled, and subtracted online. The inset shows a plot of total charge moved (Q) versus V_t for ON and OFF currents. The ON points were fitted to a sum of two Boltzmann distributions: $Q = Q_1/\{1 + \exp[-z_1(V_t - V_1)/kT]\} + Q_2/\{1 + \exp[-z_2(V_t - V_2)/kT]\}$. The fitted parameters were as follows: Q_1 = 42 fC, z_1 = 2.0 e_0, V_1 = −49 mV, Q_2 = 73 fC, z_2 = 8.6 e_0, V_2 = −39 mV; k is the Boltzmann constant, and the temperature T = 290.6 K. File, M05b. (**B**) Simulated gating currents from a single channel responding to a sudden change in potential. 1, Idealized impulses representing gating transitions scaled by the value of the transition charge. Note the presence of fluctuations even in the steady state. 2, The filtered events under "high bandwidth" conditions ($B \simeq 8\alpha_{ij}$). 3, The effect of filtering with a bandwidth comparable to the value of the transition rates. Note the reduced size of the events as indicated by the scale bar and the smearing of the individual shots. Overlapping of events limits the ability to reconstruct the original shot events. An inappropriately small bandwidth limits the amount of useful information obtainable from statistical measures of macroscopic gating current fluctuations. The autocovariance function gives an indication of this smearing effect (*13*).

D. Sigg and F. Bezanilla, Department of Physiology, School of Medicine, University of California at Los Angeles, Los Angeles, CA 90024, USA.
E. Stefani, Department of Molecular Physiology and Biophysics, Baylor College of Medicine, Houston, TX 77030, USA.

*To whom correspondence should be addressed.

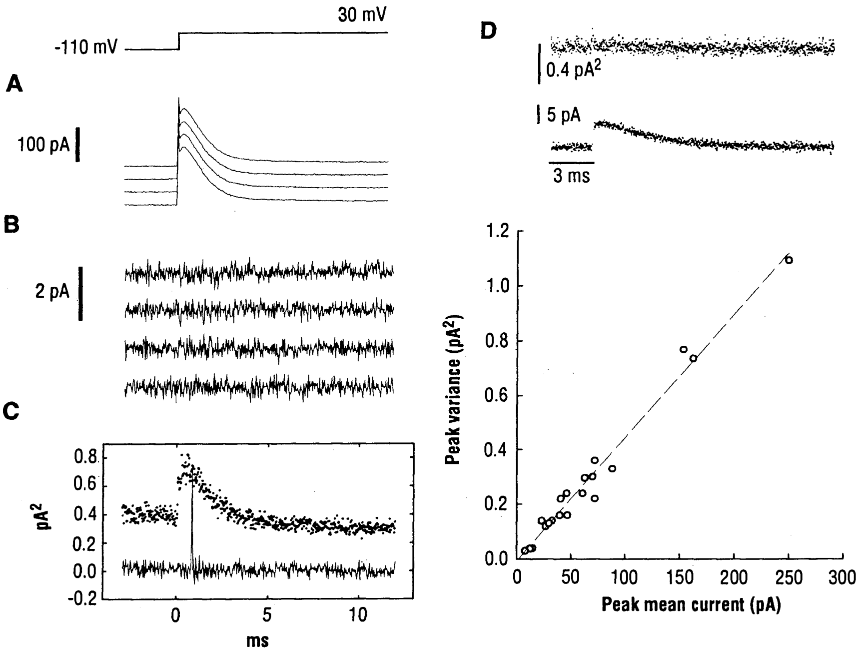

Fig. 2. Procedure for calculating the gating variance. The membrane potential pulse protocol is shown at the top left of figure. File, A20a; temperature, 17.0°C. (**A**) Sample of raw traces with no linear subtraction. Selection on the basis of absence of any unusual noise, such as that caused by seal breakdown or stretch channels, was done by eye. Remaining traces were then individually aligned with respect to the average taken over a segment in which the current had decayed to less than 5% of the maximum amplitude. Regions of different potential were aligned individually to minimize any contribution of membrane leak differences between traces. (**B**) Noise traces calculated from the formula $y_i = ½(x_i - x_{i+1})$, where x_i refer to the aligned traces. Traces y_i that exhibited excessive spikiness or slow vibrational components were discarded, as were traces offset from the zero line. (**C**) The variance (upper trace) was calculated from N traces y_i as $2[\Sigma_i(y_i - \mu_i)^2]/(N - 1)$, where μ_i is the ensemble mean of the traces y_i. The autocorrelation function (lower trace) was derived in the same manner as the variance, with the formula $C(t - t_r) = 2\Sigma_i\{[y_i(t) - \mu_i(t)][y_i(t_r) - \mu_i(t_r)]\}/(N - 1)$, where t_r is the reference time and the other symbols have the same meaning as above. The narrow spike centered around t_r is expected from a high bandwidth recording with contributions from both the shot process and random thermal noise. The width of the spike was invariant whether t_r was placed in the pre-pulse, the test pulse, or the post-pulse, and no noticeable correlation signal was obtained outside the spike that was consistently attributable to the gating process and not due to spurious forms of correlated activity (such as low-level vibrational noise or microphonics). (**D**) To indicate proper scaling of the gating noise to the amount of channel expression, we plotted peak gating variance (minus background noise) to peak gating current. Estimates were made by positioning of line cursors by eye. V_t = 10 mV, V_p = −110 mV. The traces show an example of the variance seen in an oocyte with only 5 pA of peak gating current, and it is nearly flat. Thus, nonstationary fluctuations are not a property of the injected oocyte but require expression of gating channels.

mutation in the pore region (W434F) that blocked ionic currents but had no noticeable effects on gating currents (*10*) and with a deletion of residues 6 to 46 in the NH_2-terminus (*11*) that removed N-type inactivation and charge immobilization during deactivation (*12*) (Fig. 1A). By aligning a succession of traces obtained in identical conditions and calculating the ensemble variance (Fig. 2), we obtained an estimate of the magnitude and time course of fluctuations in the gating current. The fact that the autocovariance function (*13*) had no significant component outside of the reference time (Fig. 2C), together with the finding that the maximum height of the variance scaled properly with the number of K^+ channels expressed in the membrane (Fig. 2D), provided strong evidence that the observed fluctuations are due to noise produced by the gating process of the channel.

The time course of the mean gating current during activation (ON) had an initial rising phase followed by a decay phase, as the channel relaxed to steady state during the test pulse (Fig. 3A). Correspondingly, the activation kinetics can be divided into two sequential stages, stage I and stage II. The rising phase of the ON gating current implies a sequential gating scheme in which earlier transitions (stage I) carry less charge than those occurring later (stage II) (*14*). The ON variance (Fig. 3A) also had an initial rising phase, but its peak was delayed by about 0.7 ms with respect to the peak of the ON mean. The explanation for the delay lies in the way the variance and mean differ in their charge dependence. The mean is proportional to the first power of the transition charge, whereas the variance goes as the square of the charge (*8*). Thus, when activating at a test poten-

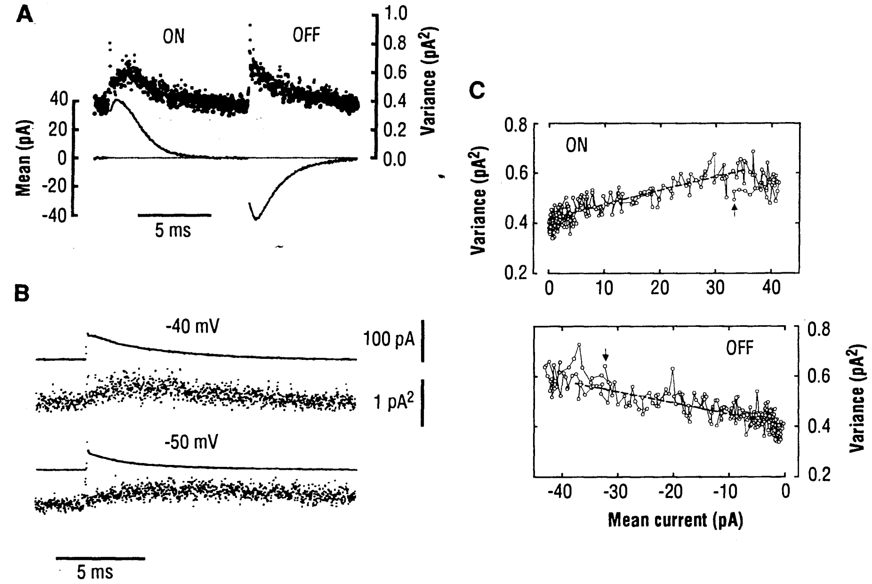

Fig. 3. Characteristics of gating current noise. (**A**) Mean (lower trace) and variance (upper trace) of activation (ON) to +10 mV for 10 ms, followed by deactivation (OFF) to −110 mV. Number of traces, 378; temperature, 17.5°C. (**B**) Mean (smooth traces) and variance for depolarizations of −40 and −50 mV after a pre-pulse to −110 mV. Temperature, 16.7°C. (**C**) Mean-variance fit (dashed line) of the decay in (A) of the ON and OFF to $Var = 2BqI - I^2/N$. The effective bandwidth $B = 1.064f_c$, appropriate for a Gaussian filter with cutoff frequency f_c (*6*). The data points are grouped as the average of pairs and are shown connected to indicate the progression in time of the plot, starting with the arrow at time zero. File, M05b.

Table 1. Results from individual gating noise experiments (listed under "File"). V_p, pre- and post-pulse potential; V_t, test pulse potential; N_{tr}, number of selected traces in calculation of variance; Var_{bas}, steady-state variance at the test potential; Q_t, total amount of ON gating charge; q_p and N_p, charge and number of gating units as fitted by the two-state irreversible model in the variance-mean plot. Average of q_p (±SE) = 2.4 (±0.12). Ig_{max}, peak current at the beginning of the decay phase; τ_p, time constant estimated from the relation $\tau_p = N_p q_p / I_{max}$; τ_o, observed time constant. The average value of τ_p/τ_o was 0.2. Dashed entries for file M04a indicate that the fit of Var_g versus I_g produces a straight line.

File	V_p:V_t (mV)	N_{tr}	Var_{bas} (pA)^2	Q_T (fC)	q_p + SD (e_0)	N_p ± SD (×10^4)	Ig_{max} (pA)	τ_p (ms)	τ_o (ms)
A20a	−110:30	350	0.36	203	1.8 ± 0.1	6.1 ± 1.0	136	0.1	1.0
A23a	−110:10	279	0.59	267	2.5 ± 0.3	5.0 ± 1.4	152	0.1	1.0
A23b	−140:10	165	0.41	178	3.3 ± 0.4	2.0 ± 0.8	178	0.2	1.2
A23c	−110:10	318	0.87	335	2.8 ± 0.2	5.3 ± 1.3	142	0.2	1.5
A23d	−110:10	397	0.24	80	1.9 ± 0.2	4.8 ± 3.3	40	0.4	1.1
F01a	−90:10	374	0.42	51	2.2 ± 0.7	2.1 ± 2.7	24	0.3	1.4
F10a	−90:10	432	0.47	130	2.6 ± 0.2	2.2 ± 0.5	60	0.2	1.3
F10f	−90:10	514	0.40	76	2.6 ± 0.3	1.3 ± 0.6	28	0.2	1.8
M04a	−110:10	186	0.73	145	2.5 ± 0.2	---	45	---	1.4
M05b	−110:10	409	0.42	103	2.2 ± 0.4	6.8 ± 14	35	0.7	1.5
M05c	−80:10	188	0.38	96	2.7 ± 0.4	2.0 ± 1.2	40	0.2	1.3
M05d	−110:10	361	0.60	147	1.9 ± 0.3	8.2 ± 9.3	67	0.4	1.1

tial (V_t) positive enough to emphasize forward rates, a delay between the peak of the variance and the peak of the mean suggested the presence of highly charged transitions occurring toward the end of the activation sequence (stage II). When V_t was less depolarized, the time between peaks of the mean and variance became longer. At −40 mV, the mean gating current started with a plateau, which was followed by a slow decay. The peak of the variance at −40 mV was not reached until the mean had decreased to about one-third of its initial value, at 3 ms. At −50 mV, the shift between peak mean gating current and peak variance was even more pronounced (Fig. 3B). An explanation for the above observations is that at these lower potentials the earlier stage I transitions are predominantly forward, whereas stage II transitions have comparable forward and backward rates producing offsetting charge movements. The result is that the contribution to the ON variance by stage II transitions becomes maximal (*15*), whereas the stage II contribution to the ON mean is reduced. Most of the contribution to the ON mean was from the more rapid stage I transitions, which contributed little to the variance because they carried less charge. These results agree with the idea that initial stage I transitions must be made of smaller shots, whereas later stage II transitions, which become slower and more spread out when pulsing to more negative potentials than +10 mV, contribute mainly to the gating variance by virtue of the large charge associated with those transitions.

Based on the assumption that upon deactivation the ion channel undergoes a series of changes that are the reverse of those that lead to activation, the deactivation (OFF) variance should reflect the movement of stage II transition charges followed by stage I transitions. Because stage II transitions generate the largest fluctuations, no rising phase should be observed in the variance. The fact that the OFF variance lacks a rising phase (*16*), in contrast with the distinct rising phase in the OFF mean, suggests that the small amount of charge carried by the first transition out of the open state (*17*) has to move relatively fast.

The stage II transitions that carry most of the gating charge were expected to make the largest contribution to the decay phase of the gating current. In order to estimate the average value of the transition charges that contribute to stage II, we plotted the gating variance as a function of the mean during the decay phase (Fig. 3C). The slope of the resulting curve corresponds to the value of the elementary event φ, which is in general time-dependent (*8*). The data points were fitted to the parabolic equation (*18*) $Var_g = 2Bq_p \cdot I_g - I_g^2/N_p$, in which Var_g is the variance, B is the 3-dB cutoff frequency for the 8-pole Bessel filter (*5*), q_p is the size the transition charge, I_g is the mean gating current, and N_p is the total number of gating subunits. The fitted parameters q_p and N_p have a simple interpretation if gating is produced by N identical and independent two-state subunits, which during activation undergo a single, irreversible transition with gating charge q. For this special case, $N_p = N$, $q_p = q$, and the estimated time constant, $\tau_p = N_p q_p / I_{max}$, is identical to the measured time constant τ_o. To test whether stage II transitions (which should have negligible backward rates at +10 mV) behave in this way, we calculated τ_p/τ_o for the experiments in Table 1. The result, $\tau_p/\tau_o = 0.2$, is a consequence of the curvature in the variance-mean plot produced by the time dependence of the elementary event φ (*8*), which has the additional effect of N_p underestimating the number of gating subunits N. We concluded that stage II transitions could not be approximated by a two-state model with independent subunits (*18*). However, the value of the elementary charge q_p fitted by the parabolic equation remains a lower estimate of q_{max}, the largest stage II transition charge (*8*). The value for q_p fitted from the ON current was 2.4 ± 0.1 elementary charges (e_0) ($n = 12$), and the value obtained from fitting the decay of the OFF was $q_p = -2.2$ $e_0 \pm 0.3$ ($n = 5$) (Table 1).

We simulated gating current fluctuations with an eight-state Markov model independently developed to fit high-resolution gating current kinetics (*19*). Comparisons of experimental data with simulation reveal that they are similar, with the peak of the variance delayed by 0.5 ms with respect to the peak of the mean gating current (Fig. 4A). Simulations for pulses to less depolarized potentials exhibited the increasing delay in peak variance as seen in Fig. 3B. As expected, the simulation exhibits very little autocovariance outside of the spike centered at t_r, even though the transitions are strongly interdependent (Fig. 4A). This is because the elementary events are sufficiently separated from one another in time to make the transition overlap terms of the autocovariance negligible. We estimated certain parameters of the eight-state model by fitting the simulated data to the irreversible two-state subunit model (Fig. 4B). The largest elementary shot charge of the model (q_{max}) was 3.5 e_0, and the fit estimated q_p = 2.85 e_0. Thus, as a tool for estimating q_{max}, the irreversible two-state model accounted for 85% of the model value. As expected from a cooperative model, τ_p measured from the simulation is a poor estimate of τ_o (τ_p = 0.14, τ_o = 1.26, τ_p/τ_o = 0.11). Correspondingly, the number of independent gating units is underestimated by 78% (N_p = 43,900).

Two different gating schemes are possible for the tetrameric (*20*) *Shaker* channel. (i) There is cooperativity between subunits that accounts for the correlations between transitions. (ii) The subunits act independently, but each undergoes multiple, correlated transitions. Given the movement of 12.4 charges per activating channel (*21*) as an upper estimate, one of four independent subunits has at most 3.1 charges to account for the observed kinetics and steady-state characteristics of the gating currents. Our results indicate that there exists at least one (*22*) transition that carries a minimum of 2.4 e_0, which leaves 0.7 e_0 to be distributed among all stage I plus the remaining stage II transitions, and this cannot be reconciled with the available data [stage I transitions alone account for about a third of the total

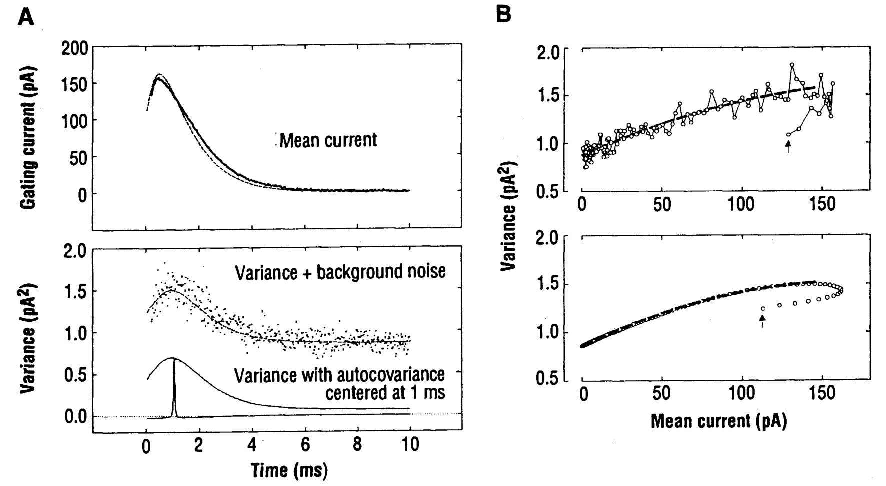

Fig. 4. Prediction of noise by eight-state Markov model. (**A**) Comparison of gating mean and variance predicted by the model (dashed line) with that of macropatch results (solid line) (file, Aug23c). The initial state of the channel was based on the equilibrium distribution at V_p. A digital Gaussian filter was used to approximate the 8-pole Bessel filter used experimentally. The digital filtering was carried out to 4 standard deviations of the impulse response function (*6*). The simulation assumed a background noise of 0.8 pA^2. Parameters of the model were adjusted to fit the experimental conditions (V_t = 10 mV, V_p = −110 mV, B = 8 kHz, T = 16.7°C). (**B**) Fits of variance versus mean of the main exponential components of simulated (lower panel) and experimental data (upper panel) to a two-state irreversible model. See text for details.

charge (*23*)]. It is therefore likely that *Shaker* subunits interact and together comprise a single gating unit in addition to being the basic unit of activation.

The results presented here place constraints on the nature of proposed gating schemes describing ion channel activation. A realistic model must incorporate at least one shot event (occurring on a much faster time scale than the filter response) that carries at least 2.4 or more elementary units of effective charge. The traditional state models [Markov models (*24*) and so-called "fractal" models (*25*)] meet this requirement, but models based purely on diffusion cannot account for the large fluctuations seen in the gating currents. Preceding the large elementary shot event (or events), there must be many transitions each carrying a small amount of charge to account for the total charge transported. The total number of stage I transitions is not known because we cannot resolve fluctuations associated with this process.

From a structural standpoint, the requirement for the four physical subunits of *Shaker* to gate as a unit implies interactions, direct or indirect, among the putative voltage-sensing regions such as the four S4 segments. If the S4 charged residues comprised most of the gating charges, large structural changes would be required to produce the measured shot charge, assuming that the electric field spanned the whole thickness of the plasma membrane (*26*). An alternative view that does not require large displacements is to assume a large number of charges or dipoles (or both) moving small distances almost simultaneously to account for the charge of stage II. Still another possibility is to consider a multitude of small structural changes, each moving a small amount of charge (stage I), that modify the local electric field, making it span a smaller region where the stage II charge moves.

REFERENCES AND NOTES

1. A. L. Hodgkin and A. F. Huxley, *J. Physiol.* **117**, 500 (1952).
2. C. M. Armstrong and F. Bezanilla, *Nature* **242**, 459 (1973).
3. G. L. Millhauser, E. E. Salpeter, R. E. Oswald, *Proc. Natl. Acad. Sci. U.S.A.* **85**, 1503 (1988); D. G. Levitt, *Biophys. J.* **66**, 489 (1989).
4. F. Bezanilla, *J. Membr. Biol.* **88**, 97 (1985).
5. F. Conti and W. Stühmer, *Eur. Biophys. J.* **17**, 53 (1989).
6. S. C. Crouzy and F. J. Sigworth, *Biophys. J.* **64**, 68 (1993).
7. The patch clamp technique measures charge movement as it appears from the outside of the membrane field. Therefore, it is impossible to individually determine either the absolute charge or the fractional field it traverses across the membrane. As a result, no distinction can be made between absolute charge displacement and dipole rearrangement, since both have units of charge times fraction of potential from the standpoint of measurement and neither is limited to integer multiples of the elementary charge unit. We label all forms of electrical rearrangement within the membrane simply as charge movement (the product of charge and fractional field) without reference to its possible origin.
8. The expression relating the variance from macroscopic gating currents to the elementary electrical events has a simple form with the assumption of high bandwidth because then the variance depends primarily on the magnitude of the elementary transition rather than on their degree of overlap (Fig. 1B). In this case, the expressions for the nonstationary mean (I_g) and variance (Var_g) of gating currents from N independent gating subunits can be obtained directly from Campbell's theorem [S. O. Rice, *Selected Papers on Noise and Stochastic Processes*, N. Wax, Ed. (Dover, New York, 1954): $I_g = N{\cdot}\Sigma_{ij} p_i \alpha_{ij} q_{ij}$ and $Var_g = N{\cdot}\Sigma_{ij} p_i 2B\alpha_{ij} q_{ij}^2$, where p_i is the probability of the channel residing in state i, α_{ij} is the rate of transition from i to j, q_{ij} is the transition charge movement, B is the effective bandwidth, and the sums are taken over all transitions. In the case of a single transition from i to j at high bandwidth and for an irreversible two-state model (for example, in the Hodgkin and Huxley model with negligible backward rates), the ratio between the variance and the mean can be used to calculate the size of the elementary event q_{ij} from $Var_g/I_g = \phi_{ij} = 2Bq_{ij}$, where ϕ_{ij} corresponds to the slope of a nonstationary plot of variance versus mean. In the more general case of a multistate gating process, the Var_g/I_g ratio ϕ is averaged over many transitions, thus $\phi = 2B(\Sigma_{ij} p_i \alpha_{ij} q_{ij}^2/\Sigma_{ij} p_i \alpha_{ij} q_{ij})$. Since the p_i's of the different states are different and do not cancel, ϕ becomes time-dependent. To simplify this analysis, backward transitions (which contribute negative values of q_{ij} to I_g) can be minimized by pulsing to membrane potentials in the saturated portion of the *Q-V* curve (Fig. 1A). Under these conditions $\phi/2B$ can be no larger than the largest transition charge, which we call q_{max}, and thus a measurement of the slope of a mean-variance plot yields a lower estimate of q_{max}.
9. Macropatch seals measuring between 7 and 20 gigohms were formed from injected *Xenopus* oocytes. We left most patches cell-attached because this tended to minimize long-term changes in current during the 10- to 20-min duration of each experiment. Solutions are in millimolar and buffered to pH 7.2. Symmetric potassium methanesulfonate (KMES) solutions that minimized the effects of pipette junction potentials were used in about half the experiments. External: 110 KMES, 2 $CaCl_2$, 10 Hepes-K; internal: 110 KMES, 10 Hepes-K, 2 K_2-EGTA. In the rest of the experiments solutions were as follows. External: 50 KCl, 75 (*N*-methyl D-glucamine)-Cl, 1.8 $CaCl_2$, 10 K-Hepes. Internal. (i) For cell-attached patches: 145 KCl, 10 K-Hepes, 5 K_2-EGTA; (ii) for excised patches: 140 (*N*-methyl D-glucamine)-glutamate, 10 (*N*-methyl D-glucamine)-Hepes, 5 (*N*-methyl D-glucamine)$_2$-EGTA. The junction potentials were measured and corrected for. The bath temperature was controlled with a Peltier unit and ranged from 16.7° to 18.3°C. Test pulses were made 500 ms apart in groups of 30, separated by four subtraction pulses done outside the range of gating charge movement, usually from 30 to 60 mV. Patches from oocytes, which were injected but did not express observable gating currents, did not exhibit nonlinear capacity components. In some cases, nonlinear resistive leak was seen during experiments and corrected. All data were filtered at 8 kHz with an 8-pole Bessel filter in series with the 4-pole Bessel filter of the patch amplifier set at 50 or 100 kHz, and digitized with a sampling rate of 40 to 125 kHz. Acquisition and analysis of all the data were done with software developed in the laboratory. Bit noise was minimized by the use of a 16-bit analog-to-digital converter, which reduces error to less than 0.005 pA^2 at even the lowest gain used. Converting integer values to floating point before calculating the variance prevented truncation error.
10. E. Perozo, R. MacKinnon, F. Bezanilla, E. Stefani, *Neuron* **11**, 1 (1993).
11. T. Hoshi, W. N. Zagotta, R. W. Aldrich, *Science* **250**, 533 (1990).
12. F. Bezanilla, E. Perozo, D. M. Papazian, E. Stefani, *ibid.* **254**, 679 (1991).
13. The autocovariance is a measure of the probability of occurrence of an event at the reference time in relation to the probability of occurrence before and after the reference time. This function has two parts. The first arises from the shape and time distribution of individual transition events, and the second from the overlap between different events (*6*). At low bandwidth the two terms may become comparable because of overlap. At high band-

width the first term predominates, greatly simplifying the analysis.

14. C. M. Armstrong and F. Bezanilla, *J. Gen. Physiol.* **63**, 533 (1974); F. Bezanilla and R. E. Taylor, in *Abnormal Nerves and Muscles as Impulse Generators*, W. J. Culp and J. Ochoa, Eds. (Oxford Univ. Press, New York, 1982), pp. 62–79.
15. The steady-state variance is expected to differ as the channel approaches equilibrium at different potentials, since its value depends on the rate and amount of charge movement of the transitions between states populated at each potential. The maximum value occurs when forward and backward rates are equal. Unfortunately, absolute values of steady-state gating variance are not readily obtained because of the difficulty of determining background noise at different potentials. The background noise is dependent on the patch characteristics, and frequently it increases with membrane polarization and the lifetime of the patch, the most probable cause being seal instability.
16. Obtaining the clean traces required for successful noise analysis occurred less frequently at very negative potentials such as −110 mV, where seal instability often produced flickering "chatter" noise, particularly at the beginning of the return pulse. Thus, we cannot with certainty discount the presence of a rising phase of the OFF variance lasting less than 0.4 ms.
17. The transition from the open state to the last closed state has been found to be relatively voltage-independent [W. N. Zagotta and R. W. Aldrich, *J. Gen. Physiol.* **95**, 29 (1990); (*26*)].
18. The classic application of nonstationary noise analysis has been to estimate the single-channel current from macroscopic ionic currents [F. J. Sigworth, *J. Physiol.* **307**, 97 (1980)]. Applied to ionic currents, it is sufficient that a single level of conductance exists in order to produce a parabolic mean-variance curve. A parabolic variance-mean curve arises if the single-channel variance has the form $var = \phi \cdot i - i^2$, where ϕ is the elementary event and is constant with time. Assuming noninteraction between channels, the relation for N channels (Var versus I) becomes $Var = \phi \cdot I - I^2/N$, which has a peak at $(N\phi/2, N\phi^2/2)$. For ionic currents, the elementary event ϕ is the single-channel current, and the peak of the parabola corresponds to an open probability of 0.5. In the case of gating currents, the requirements to apply the formula $Var = \phi \cdot I - I^2/N$ are more stringent (*6*). Activation must consist of uncorrelated transitions, implying that the channel is made up of independent two-state gating subunits that undergo irreversible transitions. Another requirement is favorable bandwidth [$(B >> \alpha)$, where α is the unimolecular rate constant governing a single subunit]. With these conditions, the elementary event has the value $\phi = 2Bq$, thus providing an estimate of the single-transition gating charge q. Gating current fluctuations cannot reach the peak of the parabola without violating the conditions of the two-state model, as it corresponds to $\alpha = B$.
19. The following linear eight-state model was developed by F. Bezanilla, E. Perozo, and E. Stefani (*26*) to account for the kinetics and voltage dependence of macroscopic gating currents in the range of −150 to 40 mV
$$C_O \underset{\beta_0}{\overset{\alpha_0}{\rightleftharpoons}} C_1 \underset{\beta_1}{\overset{\alpha_1}{\rightleftharpoons}} C_{11} \underset{\beta_1}{\overset{\alpha_1}{\rightleftharpoons}} C_{12} \underset{\beta_1}{\overset{\alpha_1}{\rightleftharpoons}} C_2 \underset{\beta_2}{\overset{\alpha_2}{\rightleftharpoons}} C_3 \underset{\beta_3}{\overset{\alpha_3}{\rightleftharpoons}} C_4 \underset{\beta_4}{\overset{\alpha_4}{\rightleftharpoons}} O$$
The equivalent of stage I in this work may include transitions between states C_0 through C_2, which has equivalent charges of 1.81 e_0 for α_0, β_0 and 1.24 e_0 for α_1, β_1. The large charge of stage II may comprise the cluster of transitions from C_2 through O with equivalent charges of 0.89 e_0 for α_2, β_2, 3.5 e_0 ($=q_{max}$) for α_3, β_3, and 0.35 e_0 for α_4, β_4.
20. R. MacKinnon, *Nature* **350**, 232 (1991).
21. N. E. Schoppa, K. McCormack, M. A. Tanouye, F. J. Sigworth, *Science* **255**, 1712 (1992).
22. It is not possible to distinguish a single event from a series of rapidly succeeding events if they take place over a much shorter time than the filter response. Thus, one event carrying 2.4 e_0 of gating charge may actually be composed of smaller events provided that they occur almost simultaneously.
23. F. Bezanilla, E. Perozo, E. Stefani, *Biophys. J.* **66**, 1011 (1994).
24. D. Colquhoun and A. G. Hawkes, *Proc. R. Soc. London* **199**, 231 (1977); E. Neher and C. F. Stevens, *Annu. Rev. Biophys. Bioeng.* **6**, 345 (1977).
25. L. S. Liebovitch, J. Fischbarg, J. P. Koniarek, I. Todorova, M. Wang, *Biochem. Biophys. Acta* **896**, 173 (1987).
26. S. R. Durrel and H. R. Guy, *Biophys. J.* **62**, 238 (1992).

27. We thank D. L. Toro for high-expression RNA and S. Krasne and D. E. Patton for reading and commenting on the manuscript. Supported by USPHS grants GM30376 and AR39874. D.S. was supported by NIH MSTP grant GM08042.

30 November 1993; accepted 1 March 1994

Enhanced Myocardial Function in Transgenic Mice Overexpressing the β_2-Adrenergic Receptor

C. A. Milano, L. F. Allen, H. A. Rockman, P. C. Dolber,
T. R. McMinn, K. R. Chien, T. D. Johnson, R. A. Bond,
R. J. Lefkowitz*

Transgenic mice were created with cardiac-specific overexpression of the β_2-adrenergic receptor. This resulted in increased basal myocardial adenylyl cyclase activity, enhanced atrial contractility, and increased left ventricular function in vivo; these parameters at baseline in the transgenic animals were equal to those observed in control animals maximally stimulated with isoproterenol. These results illustrate a useful approach for studying the effect of gene expression on cardiac contractility. Because chronic heart failure in humans is accompanied by a reduction in the number of myocardial β-adrenergic receptors and in inotropic responsiveness, these results suggest a potential gene therapy approach to this disease state.

Receptors coupled to heterotrimeric guanine nucleotide–binding proteins (G proteins), such as the adrenergic receptors, increase cellular concentrations of second messengers like adenosine 3′,5′-monophosphate (cAMP) and diacylglycerol, thereby regulating cellular function. The binding of the sympathetic neurotransmitter norepinephrine or the adrenal medullary hormone epinephrine to β-adrenergic receptors (β-ARs) in the heart stimulates adenylyl cyclase, raises the concentration of cAMP, and increases cardiac contractility. Increased secretion of catecholamines and stimulation of myocardial β-ARs are critical for augmenting cardiac function during stress.

In chronic congestive heart failure, an illness affecting more than 4 million Americans, there is impairment of the myocardial β-AR system. Failing human ventricular myocardium contains 50% fewer β-ARs and shows parallel decreases in agonist-stimulated adenylyl cyclase activity and even greater decreases in agonist-mediated inotropy (*1*). Nonreceptor-mediated stimulation of adenylyl cyclase with NaF, however, appears to be intact in the failing myocardium, and contractile responses to other agents, such as calcium or histamine, are also not impaired in the diseased myocardium (*1*). This supports the concept that impaired inotropic responsiveness in heart failure results from focal receptor defects. Therapeutic interventions involving the administration of agonists to stimulate β-ARs have an inherently limited efficacy, given the reduction in receptor targets in the diseased myocardium.

The development of transgenic technology, and emerging techniques for in vivo gene transfer (*2*), suggest a strategy for improving cardiac function by overexpressing the β-AR in the myocardium. Although transgenic mice have been reported that express, for example, the c-*myc* proto-oncogene or SV-40 T antigen affecting cardiac growth (*3*), to date few experiments have documented the ability of a transgene to significantly improve myocardial function (*4*).

C. A. Milano, Department of Surgery, Duke University Medical Center, Durham, NC 27710, USA.
L. F. Allen, Department of Medicine, Duke University Medical Center, Durham, NC 27710, USA.
H. A. Rockman and T. R. McMinn, Department of Medicine, University of California at San Diego, La Jolla, CA 92093, USA.
P. C. Dolber, Department of Pediatrics, Duke University Medical Center, Durham, NC 27710, USA.
K. R. Chien, Department of Medicine and Center for Molecular Genetics and the American Heart Association–Bugher Foundation Center for Molecular Biology, University of California at San Diego, La Jolla, CA 92093, USA.
T. D. Johnson, Department of Anesthesiology, Baylor College of Medicine, Houston, TX 77030, USA.
R. A. Bond, Department of Pharmacology, University of Houston, Houston, TX 77204, USA.
R. J. Lefkowitz, Department of Medicine and Howard Hughes Medical Institute, Duke University Medical Center, Durham, NC 27710, USA.

*To whom correspondence should be addressed.